Research Article | Submit Manuscript

Turkish Journal of Materials

Refining Microstructural Analysis in Metallurgy: Semantic Segmentation Enhanced by Post-Processing

M. F. Kalkan[1], A. Yavuz[2], N. F. Yılmaz[1,3,*]

[1] Department of Mechanical Engineering, Faculty of Engineering, Gaziantep University, 27310, Gaziantep, Türkiye

[2] Department of Metallurgical and Materials Engineering, Faculty of Engineering, Gaziantep University, 27310, Gaziantep, Türkiye

[3] Board of Trustees, Hasan Kalyoncu University, 27010 Gaziantep, Türkiye

Published: 20.10.2024

Turk. J. Mater. Vol: 9 No: 1 Page: 1-8 (2024) ISSN: 2636-8668

*Corresponding author's e-mail: nfyilmaz2@gantep.edu.tr

ABSTRACT This study investigates post-processing strategies to improve semantic segmentation models for microstructural characterization in metallurgy. Microstructural analysis is critical for understanding material properties and relies largely on expert knowledge. Deep learning algorithms have the potential for automation, but they encounter limitations such as small datasets and poor image quality. A watershed segmentation method is proposed after semantic segmentation, with a focus on the hypoeutectic Al-Si alloy. Post-processing methods were evaluated by automatically measuring the number of contours and average object area (features that could be fundamental in many microstructural images) within the study. After evaluating Euclidean, City Block, and Chebyshev distance transforms, the results demonstrate that while semantic segmentation provides high pixel accuracy, watershed segmentation enhances precision, particularly with City Block distance. Post-processed models have closer alignment with ground truth contours, indicating better segmentation. This emphasizes the importance of post-processing in improving semantic segmentation for metallurgical microstructural analysis, which allows for faster and more exact material assessments.

Keywords: Additive Manufacturing, 3D printing, Technologies, Materials.

Cite this article: M. F. Kalkan, A. Yavuz, N. F. Yılmaz. Refining Microstructural Analysis in Metallurgy: Semantic Segmentation Enhanced by Post-Processing. Turk. J. Mater. 9(1) (2024) 1-8.

1. INTRODUCTION

The broad use of deep learning has led to a significant increase in the popularity of semantic segmentation techniques, which binarize images by classifying each pixel in an image. It is frequently used, especially in daily life, in industrial fields such as automotive technologies, robotics, and video analysis. However, it has also gained popularity in medical and engineering fields in recent years. The results obtained in detecting and distinguishing the necessary elements in microscopic images of medical images and engineering materials are promising for automatically reading the images in these areas [1,2]. One of the most important factors in the successful production of engineering materials is

microstructure analysis. Using microstructural analysis, information can be obtained regarding the properties of the material and its production conditions [3]. Depending on the material production conditions, phase changes, grain boundaries, porosity, and cracks that can be observed in the microstructure affect many properties of the materials [4]. Considered from this perspective, qualitative and quantitative microstructural analyses have an important place in materials science. However, all these investigations require serious expert knowledge and opinion. For this reason, artificial intelligence applications will be a crucial key that can accelerate the process of materials science.

Artificial intelligence applications are seriously taking place in the focus of material scientists. Especially, deep learning algorithms mentioned in the microstructure of metals have illustrated significant promise in automating the analysis and classification of microstructural features [5]. Additionally, there are some studies about correlation between the material properties and automated analyzed metallic microstructures. Convolutional neural network (CNN) algorithms, a type of deep learning renowned for their effectiveness with visual data, stand out as one of the most prevalent techniques in the literature and are extensively utilized in materials research [6,7]. DeCost et al.[8] created a dataset and studied the classification of the microstructural images. They also evaluated microstructures quantitatively. Azimi et al.[5] investigated Fully Convolutional Neural Network (FCNN) architecture-based semantic segmentation to perform a pixel-wise classification for extracting the features on microstructures. They resulted in fast performance and high pixel accuracy from their provided deep learning model. Despite the development of different artificial intelligence applications that can automatically perform quantitative analysis and the increasing use of these methods, there are some limitations in these operations performed on microscopic images.

The limitations are generally addressed in applications involving microstructural images, including limited datasets, computational resources, annotation challenges and the quality of the microstructural images from the automated microstructure evaluation techniques. Among the mentioned factors, the quality of microscopic images, which is the primary data-related issue, can be attributed to various reasons [9]. These reasons can include the quality of the imaging devices used and the conditions of microscopic sample preparation. Factors such as scratches, contamination, and noise on the resulting microscopic texture may lead to inaccuracies in the learning process of the model [10]. Especially in artificial intelligence applications with pixel-based classification processes, the mentioned factors could lead to problems such as over-segmentation and under-segmentation. Over-segmentation arises when an image is inaccurately divided into smaller parts due to noise or abnormalities, whereas under-segmentation results from improperly specified borders between discrete regions, limiting the accuracy of microstructural analysis in AI-based classification systems. In recent years, some researchers have carried out studies by incorporating some image processing and segmentation methods along with deep learning models. Fotos et al. [11] proposed a model that combined the deep learning methodology and the conventional watershed segmentation, named as hybrid automated microstructural analysis. They demonstrated that their approach provided more reliable segmentation results in bimodal Ti6Al4V microstructures. Different examples were also utilized for post-processing techniques to improve the performance of segmentation [12,13]. Cheng and Lui employed the weighted composite filter to boost the efficiency of their semantic segmentation model [14]. Another study focusing on enhancing the performance of a semantic segmentation model by utilizing colorized pairwise potentials was conducted by Ratajczak et al [15].

Overlapping problems (counters in an image partially cover each other), often arising from dataset insufficiency or poor image quality, as a result of semantic segmentation, significantly impact the characterization results [16,17]. The main purpose of this study is to improve the segmentation performance of the hypoeutectic Al-Si alloy produced by die-casting with a post-processing process that can be applied automatically after semantic segmentation. For the watershed segmentation algorithm used after semantic segmentation, the commonly employed Euclidean, City block, and Chebyshev distance transformation techniques were compared on the available test data, and their performances were discussed. Watershed segmentation was automatically applied to the binary masks produced by semantic segmentation and feature extraction was performed to compare the distance transform techniques between the models. The study highlights the importance of post-processing strategies in enhancing the accuracy of semantic segmentation models used on microstructural pictures of metallic alloys. Automatic post-processing methods used after semantic segmentation have the potential to provide a more precise and efficient quantitative study of microstructures in materials research.

2. MATERIAL AND METHOD

2.1 Material

The strontium element [18], which is used in Al-Si alloys to make the Si phase thinner and more homogeneous, was added to the AlSi9 alloy at 750C to create a strontium-modified AlSi9 alloy. The melted part was kept for 30 minutes at 750 ºC after modification with addition of 300 ppm strontium. Foseco DYECOAT63 coated permanent mold was preheated at 300 ºC. The cut specimen was ground with 400 to 1200 grit SiC emery papers and polished using 1µm aluminium oxide. Microstructural images were taken at 50x magnification with using optical microscopy.

2.2 Pre-Training of Segmentation

90 cropped microscopic images of size 256x256 pixels, obtained from the same specimen, were utilized in the training, validation and test datasets. Randomly divided of 70% of microstructural images pairs to the training dataset. The remaining microscopic images were divided in half into validation and test datasets. The LabKit plugin included in the

Fiji software was used for all 90 microscopic images to prepare a binary mask for training microscopic images. Pixel intensities of all microstructural images were normalized to [0,1]. Defined datasets of training and validation were augmented with using albumentations function contains the techniques of Rotate, HorizontalFlip, VerticalFlip, RandomBrightnessContrast and ShiftScaleRotate.

2.3 Training of Segmentation Model

LinkNet architecture is one of the popular semantic segmentation architectures such as FCN [19], U-Net [20], DeepLab [21]. This deep learning architecture is preferred because it has a much lower number of parameters, easy integration, and the high performance it provides with these features [22]. LinkNet was used as architecture of semantic segmentation model which has known for its fast prediction capabilities using an encoder-decoder structure. The deep learning model based on the LinkNet architecture was implemented using the Keras API within the TensorFlow framework. The encoder and decoder layers of the prepared model consisted of filter sizes of 64 to 256 using 3x3 kernels for each. ReLu was used as an activation function of the layers. Output of the model was defined for 1 class and Sigmoid function was used for activation. Adam and binary_crossentropy were used for optimizer and loss function. Batch size was set as 8 and training happened in 50 epochs. Prepared model was executed on A100 GPU in Google Colab.

2.4 Watershed Segmentation

Ten different mask predicted with using Linknet architecture based semantic segmentation model. A median filter with 3 matrix kernel size was conducted on the predicted binary masks to reduce noise. Thresholding process was carried out to specimens using Otsu's thresholding method. Afterwards, using the morphological techniques to cleaning the noise. The application of distance transform calculated the distance of each pixel to the nearest object edge. These distances were then compared with a threshold value to identify uncertain regions. Finally, watershed segmentation was completed using the connectedComponent function. In this study, the watershed segmentation algorithm was employed with three distinct distance transforms for segmentation comparison. These were, respectively, the Manhattan Distance, Euclidean Distance, and Chebyshev Distance.

2.5 Evaluation of Models

Three different post-processing techniques were compared in this study. These techniques involved utilizing Watershed segmentation models with various distance transformation techniques. Additionally, a Linknet architecture-based semantic segmentation model was included in the comparison. Pixel accuracy and other metrics from the confusion matrix were evaluated for each model. Additionally, contours from the produced masks were counted, and their areas were calculated to compare the models.

3. RESULT AND DISCUSSION

Confusion matrices obtained from the LinkNet architecture based semantic segmentation model and different distance transformation methods using in watershed segmentation after the LinkNet model are given in Figure 1. All of the four confusion matrices resulted from the same 10 microstructural images. X-axis from these confusion matrices shows the positive and negative percentages depending on the actual label and the Y-axis shows positive and negative percentages from the predicted label. Positive pixels represent the Si phases in microstructural images and negative pixels represent the aluminum phases. Total positive pixels and total negative pixels on the actual label were counted as 29.45 % and 70.55 % in the 10 tested images. It was determined that incorrect predictions increased after the different distance transform watershed segmentation methods were used as post-processing in the model trained with LinkNet architecture. On the other hand, it was observed that correct predictions decreased in positive pixels and increased in negative pixels. It was thought that the reason for this situation may be due to the processes used to clean the noise and pollution on the masks after semantic segmentation.

Pixel accuracy, precision, recall, and F1-Score metrics are obtained from confusion matrices of each model are illustrated in Figure 2. Pixel accuracies, precision, recall, and F1-Score metrics are distributed with red, green, blue and yellow columns, respectively. There is no remarkable change in the model results. However, as seen in Figure 1, it was observed that the model developed with the LinkNet architecture, which has the highest correct prediction rate, had the highest pixel accuracy results with 0.94. Likewise, it was observed that Recall and F1-Score metrics decreased after watershed segmentation was applied. On the other hand, it should be noted that watershed segmentation models were developed to overcome the overlapping problem on microscopic masks, which is the main purpose of this study. It was observed that precision increased in masks post-processed with watershed segmentation. The precision metric is found by calculating the ratio of correctly read positive pixels to all positive read pixels. It was observed that the precision metrics obtained from the models in which watershed segmentation was applied as a post-processing process increased compared to the model in which only semantic segmentation was applied. The highest result was obtained as 0.9173 as a result of the post-processing model with watershed segmentation using City block distance transform. It was seen that the results found in other watershed segmentation and post-processing models were calculated as 0.9157 and 0.9152 in the models using Chebyshev and Euclidean distance transform.

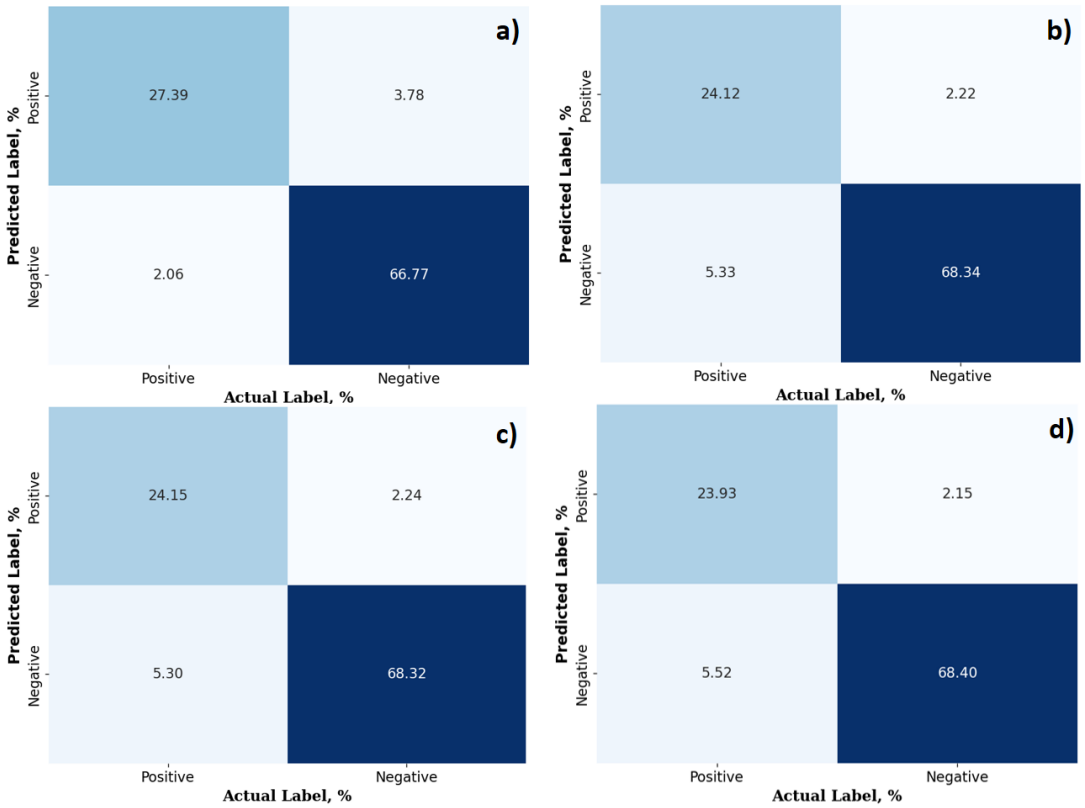

Figure 1. Confusion matrices of; a) LinkNet Model, b) LinkNet Model+Chebyshev distance transform watershed, c) LinkNet Model+Euclidean distance transform watershed, and d) City block distance transform watershed.

One part of the microstructural example of casted Al-Si alloy and its ground truth mask prepared manually are illustrated in Figure 3(a) and Figure 3(b). The image quality of the microstructural image was not seen clearly. One of the important factors affecting the semantic segmentation results is the quality of the images. Segmented mask of the microstructural example from LinkNet architecture based semantic segmentation model is given in Figure 3(c). A serious overlapping problem was detected from comparing the ground truth and LinkNet based segmented masks. While fifteen Si particles were detected in the original mask given as an example, seven Si particles were seen in the mask predicted by LinkNet. It is thought that this situation may cause errors in quantitative microstructural observations. Figures 3(d), (e) and (f) include the masks obtained as a result of applying the LinkNet+CDTW, LinkNet+EDTW and LinkNet+CBDTW post-processing methods, respectively. These masks were created by applying the LinkNet model on the predicted mask. It should be noted that the purpose of this post-processing process applied with the Watershed segmentation method is not to completely optimize it. The main purpose here is to improve the mask quality produced by the predictive semantic segmentation model. When performing a quantitative microscopic analysis, the number of grains measured, and their shapes and sizes being different will affect the characterization [23]. From this perspective, it was thought that there was an improvement in the negative effects of the original model in post-processed masks. From this perspective, it was assumed that post-processed masks improved the negative effects of the original model. It was seen that the image closest to the required mask information among the distance transform techniques used belonged to the LinkNet+CBDTW model using the city block distance transform technique. However, it was thought that it would be more appropriate to discuss the results by performing quantitative analysis on Si particles rather than objectively evaluating the results with a single sample.

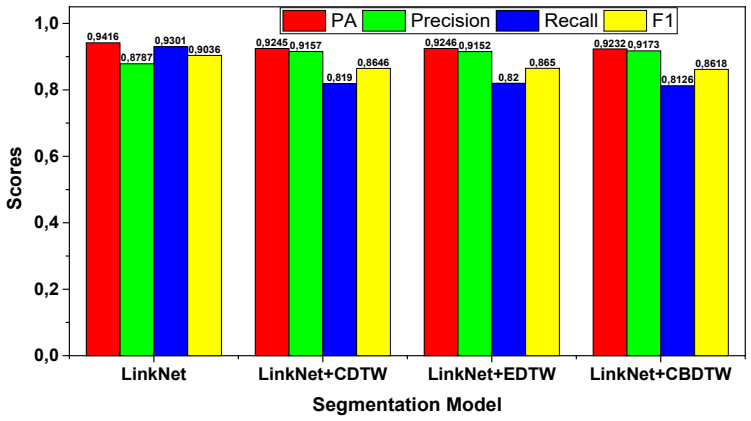

Figure 2. Comparison of pixel accuracy (PA), precision, recall, and F1-Score of all models.

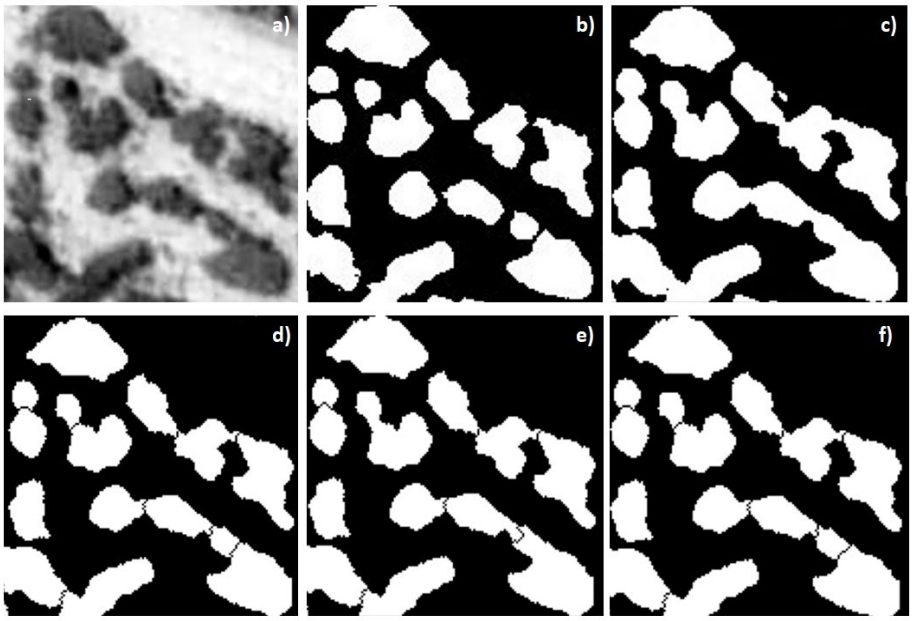

Figure 3. Images of (a) microstructural example of Al-Si alloy from dataset, (b) ground truth of microstructural example, (c) predicted mask from LinkNet, (d) predicted mask from LinkNet+CDTW, (e) predicted mask from LinkNet+EDTW, (f) predicted mask from LinkNet+CBDTW.

Table 1 shows the number of Si particles in the microscopic masks that were investigated, as well as the models' error rates. While the number of Si particles is shown in the Ground Truth data column, the other columns contain the number of Si particles as well as the error rates in the masks obtained from the models. All masks obtained from the LinkNet model showed a considerable decrease in the number of Si particles that could be counted when compared to the ground truth. One of the most likely causes of this circumstance was overlapping following semantic segmentation. The number of Si particles that could be quantified in the masks created after post-processing with different distance transform watersheds varied significantly. The number of particles in all photos increased with all three watershed segmentation approaches. It was discovered that the post-processing procedures utilized led the Si contours to be smaller than they should be, resulting in the presence of more Si particles, particularly in the predicted masks of images 4, 5, 6, 8 and 10. Among the watershed segmentation methods utilized, the city block distance transform was judged to be the most efficient for separating Si particle boundaries on the microstructure. Although some microscopic pictures had negative errors and others had positive errors, the microstructure masks created using this method had the lowest error rates. This condition was assumed to be caused by the higher Precision value given for this model in Figure 2 compared to other models.

Table 1. Number of Si Particles (NOS) and errors produced by different models.

Image No	NOS by Ground Truth	NOS by LinkNet	NOS by CDTW	NOS by EDTW	NOS by CBDTW
1	52	41 Error: -21.15 %	47 Error: -9.62 %	46 Error: -11.54 %	44 Error: -15.38 %
2	31	23 Error: -25.81 %	28 Error: -9.68 %	28 Error: -9.68 %	27 Error: -12.90 %
3	53	32 Error: -39.62 %	38 Error: -28.30 %	46 Error: -13.21 %	47 Error: -11.32 %
4	55	41 Error: -25.45%	62 Error: 12.73 %	59 Error: 7.27 %	58 Error: 5.45 %
5	31	24 Error: -22.58%	37 Error: 19.35 %	36 Error: 16.13 %	31 Error: 0.0 %
6	88	70 Error: -20.45 %	109 Error: 23.86 %	90 Error: 2.27 %	78 Error: - 11.36 %
7	34	24 Error: -29.41 %	33 Error: - 2.94 %	36 Error: 5.88 %	34 Error: 0 %
8	73	61 Error: -16.44 %	93 Error: 27.39 %	100 Error: 36.99 %	84 Error: 15.07 %
9	51	33 Error: -35.29 %	43 Error: -15.68 %	41 Error: - 19.61 %	44 Error: -13.73 %
10	69	58 Error: -15.94 %	70 Error: 1.45 %	74 Error: 7.25 %	76 Error: 10.15%

Table 2 is given to make assessment on the performance of the watershed segmentation as post-processing for semantic segmentation models. The calculated average area of the Si particles and the error rates of the prepared models are shown in Table 2. Areas of Si particles were calculated in pixel unit. Error rates were calculated using the areas of Si particles from the ground truth masks. It was detected that number of predicted contours from the basic LinkNet model less than the ground truth masks in Table 1. Due to the presence of overlapping in the masks, it was observed that the average Si particle areas in the predicted masks from the LinkNet model were higher. The increment on the average areas from the predicted masks were found in between the 16% to 37.8 %. It is believed that areal measurement at the given levels has a significant impact on microstructural characterization. Following watershed segmentation, the average areas of Si particles in the masks of all microstructural images abated. The model with the most irregular error rates was found as LinkNet+CDTW within the distance transformation techniques used post-processed models. The performance of the masks predicted from the LinkNet+EDTW model was found better than the LinkNet+CDTW from the obtained average areas in microstructural masks. Despite this, it was observed that the specified model had an error rate of over 10% in five of ten masks it predicted. The most effective model was identified as LinkNet+CBDTW in Table 1, which also had the maximum precision according to the confusion matrix. Apart from three microstructural masks generated from the city block distance transform approach used in watershed segmentation, error rates ranged within the negative or positive 10%.

Table 2. Average area of Si particles and errors produced by different models.

Image No	AAS by Ground Truth	AAS by LinkNet	AAS by CDTW	AAS by EDTW	AAS by CBDTW
1	396.84	472.20 Error: 18.99 %	354.16 Error: -10.75 %	356.49 Error: -10.17 %	374.80 Error: -5.55 %
2	398.61	465.75 Error: 16.84 %	408.18 Error: 2.40 %	406.59 Error: 2.00 %	422.94 Error: 6.10 %
3	292.61	357.51 Error: 22.18 %	350.05 Error: 19.63 %	293.53 Error: 0.32 %	317.58 Error: 8.54 %
4	388.10	464.87 Error: 19.78%	295.73 Error: -23.80 %	317.69 Error: -18.14 %	317.87 Error: -18.09 %
5	657.84	809.85 Error: 23.11%	460.01 Error: -30.08 %	474.35 Error: -27.89 %	550.09 Error: -16.38 %
6	183.94	227.91 Error: 23.90%	138.17 Error: -24.88 %	155.54 Error: -15.44 %	177.81 Error: -3.33 %
7	454.04	607.63 Error: 33.83%	474.08 Error: 4.41 %	430.31 Error: -5.23 %	441.21 Error: -2.83 %
8	276.04	328.73 Error: 19.09 %	196.63 Error: -28.76 %	184.43 Error: -33.19 %	237.92 Error: -13.81 %
9	380.46	485.78 Error: 27.68 %	371.34 Error: -2.39 %	394.41 Error: 3.67 %	410.84 Error: 7.98 %
10	164.30	226.41 Error: 37.81 %	170.40 Error: 3.71 %	174.47 Error: 6.19 %	170.31 Error: 3.66 %

Total number of contours in 10 images are given in Figure 4(a). A total of 407 contours were detected in the masks belonging to the microscopic images estimated with the prepared LinkNet model. However, 537 contours were found in manually prepared ground truth masks. Although the images trained with the LinkNet model initially had a 25% error rate in the number of contours, it was observed that applying the post-processing process reduced these error rates by 2% to 5%. More contour numbers were obtained than ground truth when the overlapping problem was attempted to be solved using post-processing methods under CDTW and EDTW models. It was thought that the contours were incorrectly divided in the specified models. It was observed that the closest result was in the masks estimated with the LinkNet+CBDTW model by detecting 523 contours. The average areas of Si particles in all images are shown in Figure 4(b). It was observed that the results approached the average area obtained from ground truth masks in all three post-processing techniques. Training with the LinkNet architecture resulted in an error margin of approximately 24%. Upon the application of post-processing, a notable decrease in the error rate was observed. The analysis revealed that the images generated using the LinkNet + CDTW and LinkNet + EDTW algorithms exhibited error rates of 10.3% and 11.2% respectively. The LinkNet+CBDTW model yielded the most favorable outcomes, achieving approximately 4% in terms of the number of contours.

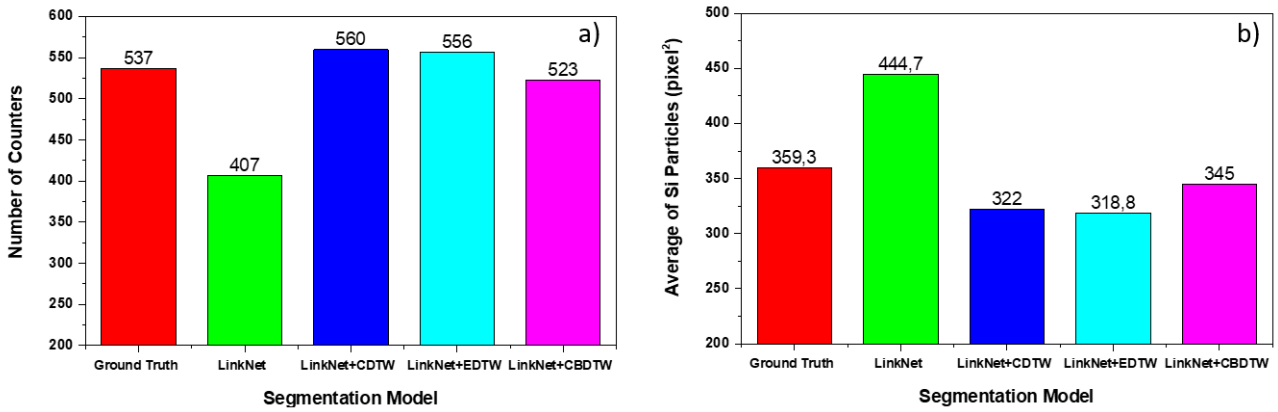

Figure 4. Total NOC (a) and average AAS (b) bar graphs for ground truth and different models.

It was observed that the developed method performed better than the semantic segmentation model after training on the test dataset. One of the most important advantages here is that the combined contours can be distinguished from each other after segmentation. It is known that contours can be distinguished better in instance segmentation algorithms rather than traditional semantic segmentation models. It was seen that the necessary improvements regarding contour could be achieved with the post-processing method presented in this study [14]. However, it should not be forgotten that this post-processing process does not involve any learning and that presetting must be made for the dataset to be used. This method is not a model that can be used instead of an existing machine learning or deep learning algorithm, but rather to improve the results of an existing semantic segmentation model. There are various methods used in this sense in the literature in recent years [12,14]. It is seen that the developed methods improve the artificial intelligence results in the datasets in which they are used.

4. CONCLUSION

This work highlights the usefulness of post-processing operations in semantic segmentation models created using deep learning approaches for metallic microstructural pictures. One of its most significant advantages is that the available post-processing processes can be performed automatically on the dataset to be used. This will allow for more precise and faster quantitative assessments of the microstructure during the material development process. However, semantic segmentation applications may provide performance improvements over more expensive methods such as instance segmentation. Different distance transformation strategies were employed in the watershed methodologies used. The semantic segmentation model without post-processing demonstrated the highest pixel accuracy, recall, and F1-Score values. However, post-processing with watershed segmentation resulted in enhanced precision values. The precision value was deemed to be particularly essential in masks designed for microscopic investigations. It was discovered that the strategies utilized might solve the overlapping problem in masks estimated with the semantic segmentation model. It was determined that the city block distance transform technique provides a more effective performance with watershed segmentation, especially in the microstructural images of the Al-Si alloy used. However, it should also be noted that the effects of the applied methods will vary depending on different datasets. It is expected that this study will take its place in the literature in terms of showing the effects of a post-processing process to be applied to promising image-based artificial intelligence techniques in the field of metallography.

REFERENCES

[1] F. Jiang, A. Grigorev, S. Rho, Z. Tian, Y. Fu, W. Jifara, K. Adil, S. Liu, Medical image semantic segmentation based on deep learning, Neural Comput. Appl. 29 (2018) 1257–1265.

[2] H. Hwang, S.M. Choi, J. Oh, S.-M. Bae, J.-H. Lee, J.-P. Ahn, J.-O. Lee, K.-S. An, Y. Yoon, J.-H. Hwang, Integrated application of semantic segmentation-assisted deep learning to quantitative multi-phased microstructural analysis in composite materials: Case study of cathode composite materials of solid oxide fuel cells, J. Power Sources. 471 (2020) 228458.

[3] J. Fu, S. Qu, J. Ding, X. Song, M.W. Fu, Comparison of the microstructure, mechanical properties and distortion of stainless steel 316 L fabricated by micro and conventional laser powder bed fusion, Addit. Manuf. 44 (2021) 102067.

[4] W.R. Osório, L.C. Peixoto, M. V Canté, A. Garcia, Microstructure features affecting mechanical properties and corrosion behavior of a hypoeutectic Al–Ni alloy, Mater. Des. 31 (2010) 4485–4489.

[5] S.M. Azimi, D. Britz, M. Engstler, M. Fritz, F. Mücklich, Advanced steel microstructural classification by deep learning methods, Sci. Rep. 8 (2018) 2128.

[6] C. Herriott, A.D. Spear, Predicting microstructure-dependent mechanical properties in additively manufactured metals with machine-and deep-learning methods, Comput. Mater. Sci. 175 (2020) 109599.

[7] M. Warmuzek, M. Żelawski, T. Jałocha, Application of the convolutional neural network for recognition of the metal alloys microstructure constituents based on their morphological characteristics, Comput. Mater. Sci. 199 (2021) 110722.

[8] B.L. DeCost, T. Francis, E.A. Holm, Exploring the microstructure manifold: image texture representations applied to

ultrahigh carbon steel microstructures, Acta Mater. 133 (2017) 30–40.
[9] J. Jung, J. Na, H.K. Park, J.M. Park, G. Kim, S. Lee, H.S. Kim, Super-resolving material microstructure image via deep learning for microstructure characterization and mechanical behavior analysis, Npj Comput. Mater. 7 (2021) 96.
[10] P. Warren, N. Raju, A. Prasad, M.S. Hossain, R. Subramanian, J. Kapat, N. Manjooran, R. Ghosh, Grain and grain boundary segmentation using machine learning with real and generated datasets, Comput. Mater. Sci. 233 (2024) 112739.
[11] G. Fotos, A. Campbell, P. Murray, E. Yakushina, Deep learning enhanced Watershed for microstructural analysis using a boundary class semantic segmentation, J. Mater. Sci. 58 (2023) 14390–14410.
[12] G. Zhu, R. Wang, Y. Liu, Z. Zhu, C. Gao, L. Liu, N. Sang, An adaptive post-processing network with the global-local aggregation for semantic segmentation, IEEE Trans. Circuits Syst. Video Technol. (2023).
[13] D. Kochanov, F.K. Nejadasl, O. Booij, Kprnet: Improving projection-based lidar semantic segmentation, ArXiv Prepr. ArXiv2007.12668. (2020).
[14] X. Cheng, H. Liu, A novel post-processing method based on a weighted composite filter for enhancing semantic segmentation results, Sensors. 20 (2020) 5500.
[15] R. Ratajczak, C. Crispim, B. Fervers, E. Faure, L. Tougne, Semantic segmentation post-processing with colorized pairwise potentials and deep edges, in: 2020 Tenth Int. Conf. Image Process. Theory, Tools Appl., IEEE, 2020: pp. 1–6.
[16] R. Usamentiaga, D.G. Lema, O.D. Pedrayes, D.F. Garcia, Automated surface defect detection in metals: A comparative review of object detection and semantic segmentation using deep learning, IEEE Trans. Ind. Appl. 58 (2022) 4203–4213.
[17] G. Roberts, S.Y. Haile, R. Sainju, D.J. Edwards, B. Hutchinson, Y. Zhu, Deep learning for semantic segmentation of defects in advanced STEM images of steels, Sci. Rep. 9 (2019) 12744.
[18] M.R.S. Ganesh, N. Reghunath, M. J. Levin, A. Prasad, S. Doondi, K. V Shankar, Strontium in Al–Si–Mg alloy: a review, Met. Mater. Int. (2022) 1–40.
[19] J. Long, E. Shelhamer, T. Darrell, Fully convolutional networks for semantic segmentation, in: Proc. IEEE Conf. Comput. Vis. Pattern Recognit., 2015: pp. 3431–3440.
[20] O. Ronneberger, P. Fischer, T. Brox, U-net: Convolutional networks for biomedical image segmentation, in: Med. Image Comput. Comput. Interv. 2015 18th Int. Conf. Munich, Ger. Oct. 5-9, 2015, Proceedings, Part III 18, Springer, 2015: pp. 234–241.
[21] L.-C. Chen, G. Papandreou, I. Kokkinos, K. Murphy, A.L. Yuille, Deeplab: Semantic image segmentation with deep convolutional nets, atrous convolution, and fully connected crfs, IEEE Trans. Pattern Anal. Mach. Intell. 40 (2017) 834–848.
[22] A. Chaurasia, E. Culurciello, Linknet: Exploiting encoder representations for efficient semantic segmentation, in: 2017 IEEE Vis. Commun. Image Process., IEEE, 2017: pp. 1–4.
[23] M. Zhang, J. Wang, B. Wang, C. Xue, X. Liu, Quantifying the effects of Sc and Ag on the microstructure and mechanical properties of Al–Cu alloys, Mater. Sci. Eng. A. 831 (2022) 142355.